Atmospheric
Chemistry
and Physics
Discussions

Multi-generation Chemical Aging of α-Pinene Ozonolysis Products by Reactions with OH

Ningxin Wang[1], Evangelia Kostenidou[2,3], Neil M. Donahue[1] and Spyros N. Pandis[1,2,3]

[1]Department of Chemical Engineering, Carnegie Mellon University, Pittsburgh
[2]Department of Chemical Engineering, University of Patras, Patra, Greece
[3] Institute of Chemical Engineering Sciences (ICE-HT), FORTH, Patra, Greece

Abstract

Secondary organic aerosol (SOA) formation from volatile organic compounds (VOCs) in the atmosphere can be thought of as a succession of oxidation steps. The production of later-generation SOA via continued oxidation of the first-generation products is defined as chemical aging. This study investigates aging in the α-pinene ozonolysis system with hydroxyl radicals (OH) through smog chamber experiments. The first-generation α-pinene ozonolysis products were allowed to react further with OH formed via HONO photolysis. After an equivalent of 2-4 days' of typical atmospheric oxidation conditions, homogeneous OH oxidation of the α-pinene ozonolysis products resulted in a 20-40 % net increase of the SOA for the experimental conditions used in this work. A more oxygenated product distribution was observed after aging based on the increase in aerosol atomic oxygen to carbon ratio (O:C) by up to 0.04. Experiments performed at intermediate relative humidity (RH) of 50 % showed no significant difference in additional SOA formation during aging compared to those performed at low RH of less than 20 %.

1. Introduction

Anthropogenic activities such as fuel combustion as well as biogenic sources such as emissions from vegetation can introduce particles and particle precursors into the atmosphere. In most areas, about half of the submicron aerosol mass on average is composed of organic compounds (Zhang et al., 2007). Organic particles directly emitted to the atmosphere are traditionally defined as primary organic aerosol (POA), while those formed through atmospheric

Atmospheric
Chemistry
and Physics
Discussions

29   reactions and condensation of species with corresponding volatility are secondary (SOA).

30   Atmospheric aerosols represent a significant risk to human health by causing respiratory problems

31   and heart attacks (Davidson et al., 2005; Pope et al., 2009). At the same time these particles

32   influence the climate of our planet (Intergovermental Panel on Climate Change, 2007).

33   Oxygenated OA with a high oxygen to carbon ratio (O:C) is often the most important

34   component of ambient OA suggesting the importance of atmospheric chemistry in the formation

35   and processing of OA (Zhang et al., 2007). Most laboratory studies of SOA formation so far have

36   focused on the first stage of reactions involving the target precursor reacting with the chosen

37   oxidant. In the atmosphere, organic vapors and particles interact with oxidants for days and

38   therefore successive oxidation processes are inevitable.

39   Chemical aging refers to the subsequent stages of SOA formation and evolution due to the

40   production of later-generation products via oxidation of first-generation products by oxidants such

41   as OH free radicals (Donahue et al., 2006; Henry et al., 2012). Previous studies have explored

42   various forms of aging, including heterogeneous reactions of oxidants and aerosols (George et al.,

43   2008), oligomerization (Kalberer et al., 2006), photolysis of either gas or condensed-phase

44   products (Henry and Donahue, 2012), and homogeneous gas-phase oxidation by OH (Donahue et

45   al., 2012). Homogeneous gas-phase oxidation reactions appear to be in general much faster than

46   heterogeneous reactions, due to diffusion limitations of the latter (Lambe et al., 2009). The first-

47   generation oxidation reactions of most SOA precursors convert much less than 50 % of the

48   precursor to SOA, leaving more than half of the carbon still in the gas-phase. Additional oxidation

49   of these vapors can potentially contribute additional and more oxygenated SOA components.

50   These later-generation reactions have been proposed to be a major missing step connecting

51   chamber studies to field measurements.

52   Zeroth order parameterizations have been developed to model the chemical aging of semi-

53   volatile POA emissions in chemical transport models (Robinson et al., 2007). CTMs using these

54   schemes show improved performance in urban areas such as Mexico City (Tsimpidi et al., 2011),

55   but tend to over-predict OA in areas such as the southeastern United States where biogenic VOCs

56   dominate if chemical aging is assumed to be a major source of additional SOA (Lane et al., 2008).

57   As a result, the importance of aging of biogenic SOA as a source of SOA mass concentration

58   remains an issue of debate.

Atmospheric
Chemistry
and Physics
Discussions

59   The ozonolysis of α-pinene ($C_{10}H_{16}$) is considered one of the most important global SOA

60   sources (Griffin et al., 1999). The system has been well characterized through smog chamber

61   experiments where researchers quantified its SOA yields under different conditions, explored the

62   reaction pathways and mechanisms, and identified its product distributions. Recent studies suggest

63   that there is significant potential for additional SOA formation from homogeneous gas-phase aging

64   by OH of the first-generation α-pinene oxidation products. Major identified products existing in

65   gas phase such as pinonaldehyde and pinonic acid can serve as SOA precursors and further react

66   with OH. Pinonaldehyde reacts with OH, with SOA mass yields up to 5 % under low-NO_x

67   conditions and 20 % under high-NO_x conditions (Chacon-Madrid et al., 2013). Müller et al. (2012)

68   demonstrated the formation of 1,2,3-butanetricarboxylic acid (MBTCA), an SOA product of low

69   volatility identified in α-pinene ozonolysis, through the gas-phase OH oxidation of pinonic acid.

70   They reported an experimental yield of 0.6 % for MBTCA from the gas-phase OH oxidation of

71   pinonic acid, accounting for about 10 % of the total SOA formed. The proposed formation

72   mechanisms of MBTCA is a classic example of semi-volatile precursors going through oxidation

73   and forming products of lower volatility.

74   The Multiple Chamber Aerosol Chemical Aging Study (MUCHACHAS) explored the gas-

75   phase OH aging effects of the α-pinene ozonolysis products via experiments performed in four

76   different smog chambers (Donahue et al., 2012). They were able to isolate the aging effect by

77   using different OH sources (HOOH photolysis, HONO photolysis, TME ozonolysis), light sources

78   (sunlight, quasi-solar lamps, 350 nm UV lamps), and chambers of different design in size and

79   material (Teflon and aluminum). Almost in all experiments, additional formation of SOA (up to

80   55 %) and a more oxidized product distribution (increasing O:C) were observed after aging.

81   However, in one of the chambers, strong UV photolysis led to decreasing SOA mass

82   concentrations in experiments with low to moderate OH levels, [OH] $\leq 2\times10^6$ molecules cm^{-3}

83   (Henry and Donahue, 2012). These authors concluded that chemical aging involves a complex set

84   of interacting processes with competing functionalization (conserved C number with products of

85   lower volatility and higher oxidation states) and fragmentation (cleavage of C-bond with products

86   over a wide volatility range and higher oxidation states) of the various organic compounds. A 2D-

87   volatility basis set (2D-VBS) simulation based on these two pathways and a branching ratio

88   between them showed that homogeneous OH aging can potentially more than double the α-pinene

89   SOA mass concentration, after about a day's equivalent of typical atmospheric oxidation

Atmospheric
Chemistry
and Physics
Discussions

90   conditions. Uncertainties such as "ripening" during which SOA volatility evolves but its mass

91   remains constant, UV photolysis and heterogeneous OH uptake can further complicate the aging

92   process.

93   Qi et al. (2012) also explored aging of the α-pinene ozonolysis system through smog

94   chamber experiments using HOOH as an OH source and studied the UV photolysis effect. They

95   observed a 7.5 % increase in the SOA volume concentration and an increase of 0.03 in the O:C

96   after aging. Minimum photolysis effect was reported for these experiments.

97   One complication of chamber experiments is the interaction of particles with chamber

98   walls. The wall-loss rate of particles is a function of particle size, charge distribution, chamber

99   geometry, turbulence, and electric field within the chamber (Crump and Seinfeld, 1981). In order

100 to quantify SOA yields from chamber experiments, it is important to correct for particle wall loss.

101 Recent findings that organic vapors in the chamber can be directly lost to the Teflon walls as well

102 further complicate the wall-loss correction process (Matsunaga and Ziemann, 2010; Zhang et al.,

103 2014). Krechmer et al. (2016) measured the loss rate of vapors formed in the chamber and found

104 the corresponding timescale to be 7-13 min. Ye et al. (2016) determined the vapor wall-loss

105 timescale in the Carnegie Mellon chamber used in this work to be around 15 min for semi-volatile

106 organic compounds.

107   Despite the consensus from the aforementioned chamber studies that gas-phase OH aging

108 of α-pinene ozonolysis products can contribute to additional SOA formation, there lacks

109 consistency in the extent to which the additional mass can form for different OH exposures. Part

110 of the problem is that the estimated amount of additional SOA formed from these long-lasting

111 aging experiments can be extra sensitive to the particle and the vapor wall-loss correction methods

112 deployed. The uncertainties at the end of a 10-hour long aging experiment during which most

113 particles are lost to chamber walls and the measured suspended mass is low can be relatively high.

114 In this work, we aim to quantify the additional SOA formed during the aging step comparing

115 measurements from a suite of instrumentation. We adopt a size-dependent particle wall-loss

116 correction method and develop a procedure to better constrain the associated errors. We also

117 attempt to constrain the vapor loss using both theoretical calculations and measurements.

118

119

120

Atmospheric
Chemistry
and Physics
Discussions

2. Experimental approach

We conducted experiments in a 12 m^3 Teflon (Welch Fluorocarbons) smog chamber at Carnegie Mellon University (CMU). The reactor was suspended in a temperature-controlled room with walls covered with UV lights (GE 10526 and 10244). Prior to each experiment, we flushed the chamber overnight with purified air under UV illumination to remove any residual particles and gas-phase organics. We generated purified air by passing ambient air through a high-efficiency particulate air (HEPA) filter to remove particles, an activated carbon filter to remove any organics, a Purafil filter to remove NO$_x$, and finally a silica gel filter, keeping relative humidity (RH) below 5 % in the chamber before each experiment.

We pumped an ammonium sulfate solution (1 g L^{-1}) into the chamber at the beginning of each experiment through an atomizer (TSI, model 3076) at a constant rate of 90 mL h^{-1} to produce droplets. The droplets passed through a diffusion dryer and a neutralizer to produce dry ammonium sulfate seed particles. We injected seeds with a number mode size of 110 nm until they reached a number concentration of 2×10^4 cm^{-3}, resulting in an initial seed mass concentration of around 40 μg m^{-3} and a surface area concentration of up to 1000 μm^2 cm^{-3}. Typical organic vapors with a molar weight of 250 g mol^{-1} thus had an initial collision frequency with these seeds of 0.01 s^{-1}. We injected α-pinene (Sigma-Aldrich, ≥ 99 %) into the chamber using a septum injector with purified air as carrier flow. We generated ozone using a corona-discharge ozone generator (AZCO, HTU500AC) to initiate the ozonolysis reaction. We prepared a fresh HONO solution in a bubbler by adding a 4.9 g L^{-1} sulfuric acid solution to a 6.9 g L^{-1} sodium nitrite solution. We then turned on the UV lights to start the photo-dissociation of HONO, producing OH.

At the end of each experiment, we injected additional ammonium-sulfate seeds into the chamber using the same method with a more concentrated solution (5 g L^{-1}) in order to characterize the particle wall-loss rates a second time.

We added butanol-d9 (Cambridge Isotope Laboratories, 98 %) into the chamber through the septum injector as an OH tracer before the reaction started and used the method described in Barmet et al. (2012) to calculate the OH produced by HONO photolysis. The OH concentration in these experiments was around 2.4×10^7 molecules cm^{-3} for the first hour, then dropped to around 5×10^6 molecules cm^{-3} afterwards.

Atmospheric
Chemistry
and Physics
Discussions

150   We performed experiments at both low RH of less than 20 % and intermediate RH of 50 %.

151   To add water vapor to the chamber, we used a stream of purified air to carry ultrapure water

152   (Millipore water purification system) in a bubbler into the chamber before the introduction of seeds.

153   We measured the particle size distribution using a TSI Scanning Mobility Particle Sizer,

154   SMPS (classifier model 3080; CPC model 3010 or 3772), and the particle composition and mass

155   spectrum of the OA with an Aerodyne High Resolution Time-of-flight Aerosol Mass Spectrometer

156   (HR-Tof-AMS). We monitored the concentrations of α-pinene and butanol-d9 using a Proton

157   Transfer Reaction-Mass Spectrometer (PTR-MS, Ionicon), the ozone concentration using a Dasibi

158   1008 ozone monitor (ICE: Teledyne 400E), and NO_x (NO + NO_2) levels using a Teledyne API

159   NO_x Analyzer 200A (ICE: Teledyne T201). We held the chamber temperature constant at 22 ºC

160   throughout all experiments. We list the initial conditions of the experiments performed for this

161   work in Table 1.

162

163   **3. Data analysis**

164   **3.1 SOA yields**

165   The SOA mass yield, Y, is a metric of the ability of a gaseous precursor to form SOA, and

166   is defined as $Y = C_{SOA}/\Delta VOC$, where C_{SOA} is the produced SOA mass concentration (in µg m^{-3})

167   and ΔVOC the amount of the VOC precursor (α-pinene in this case) reacted (in µg m^{-3}). To

168   separate the effect of aging on SOA mass concentration, we define a first-generation SOA mass

169   yield, $Y_1 = C_{SOA,1}/\Delta VOC$, and a second-generation SOA mass yield, $Y_2 = C_{SOA,2}/\Delta VOC$. $C_{SOA,1}$ and

170    $C_{SOA,2}$ are the concentrations of SOA formed before, and after aging with hydroxyl radicals. All

171   α-pinene reacts away during the first stage and thus ΔVOC for the second stage is the same as the

172   initial α-pinene concentration in the chamber.

173

174   **3.2 Particle wall-loss correction**

175   In this work, we try to reduce the uncertainties in the estimated SOA mass concentration

176   associated with the particle wall-loss correction. This uncertainty can be significant due to two

177   aspects of these aging experiments: the evolution of the particle size distribution and the duration

178   of the experiments. In these aging experiments, where particles grow by condensation and

179   coagulation for several hours, the particle size distribution can potentially shift, covering a wide

180   size range over the course of an experiment. Particle wall losses are size dependent, and this shift

Atmospheric
Chemistry
and Physics
Discussions

181   can introduce significant errors if a constant loss rate constant is assumed. To minimize these

182   problems, we adopted a size-dependent particle wall-loss correction method where we determined

183   the particle wall-loss rate constant, k, at each particle size, D_p.

184

185   **3.2.1 Determination of particle wall-loss rate constants**

186   The size-dependent particle wall-loss correction method (Keywood et al., 2004; Ng et al.,

187   2007; Loza et al., 2012; Nah et al., 2016) adopted in this work is based on the SMPS-measured

188   particle size distribution. At each particle size bin i, the first-order particle wall-loss rate constant

189   k, can be determined as the slope of the following equation:

190

191   $$\ln[N_i(t)] = -k_i t + Q \qquad (1)$$

192

193   where $N_i(t)$ is the SMPS-measured aerosol number concentration at size bin i and Q is an arbitrary

194   constant. Applying Eqn. 1 across the entire SMPS-measured particle size range, we obtain the

195   particle wall-loss rate constant function, $k(D_p)$.

196   To determine the $k(D_p)$ profile, we utilized the initial four-hour ammonium sulfate seed

197   wall-loss period for each experiment. Since k may also vary with time (McMurray and Rader,

198   1985), we determined a second $k(D_p)$ profile for each experiment using the ammonium sulfate

199   seed wall-loss period at the end. It is important to ensure that the k's, especially at sizes where the

200   majority of SOA mass is distributed, remain the same over the course of each experiment.

201   The $k(D_p)$ values calculated (with an $R^2 > 0.5$) based on SMPS measurements of the seed

202   distribution from this work usually only cover particle size range of 30-300 nm due to the lack of

203   particles at either end of the particle size distribution. To determine the $k(D_p)$ for $D_p < 30$ nm, we

204   use a simple log-linear fit of k's from 30-50 nm and back extrapolate it to 10 nm. To determine

205   $k(D_p)$ for $D_p > 300$ nm, we assume that the constant is practically the same in the 300-600 nm

206   range. We confirmed this with additional seed-only experiments where there were enough particles

207   at that size range (Wang et al., 2017). We then applied the complete $k(D_p)$ profile to correct for

208   the particle number and mass concentration. Details regarding the wall-loss profiles in the CMU

209   chamber and the execution of the size-dependent particle wall-loss correction for this work can be

210   found in Wang et al. (2017).

211

3.2.2 Correction of SMPS measurements

The corrected particle number concentration at each size bin i, $N_i(t)$, can be calculated numerically,

$$N_i(t) = \mathrm{N}_i^m(t) + k_i \int_0^t \mathrm{N}_i^m(t)dt, \qquad (2)$$

from the measured values $\mathrm{N}_i^m(t)$ and the $k(D_p)$ corresponding to the size bin i, k_i.

For closed systems in which coagulation is slow, the particle wall-loss corrected number concentration should be constant. In order to evaluate how well the correction works, we define the parameter: $\varepsilon_N = 2\sigma_{N_s}/\overline{N_s}$, where σ_{N_s} is the standard deviation of the particle wall-loss corrected number concentration for the seed wall-loss periods and $\overline{N_s}$ the average. Similarly, we define $\varepsilon_V = 2\sigma_{N_s}/\overline{V_s}$ based on the particle wall-loss corrected volume concentration for the two seed wall-loss periods. Only when all four values, ε_N and ε_V for both the initial and the final seed periods, are less than 5 % do we deem the particle wall-loss correction valid for that individual experiment. Experiments in which these criteria were not met were not included in the analysis.

To calculate the mass concentration of the formed SOA, C_{SOA}, during the course of an experiment, we treated the particle wall-loss corrected aerosol volume concentration $V(t)$ differently before and after its maximum, V_{max}. For

$$\mathrm{t} < t_{V_{max}}, C_{SOA}(t) = (V(t) - V_s)\rho_{SOA},$$
$$\mathrm{t} \geq t_{V_{max}}, C_{SOA}(t) = [V(t) - V_s\frac{V(t)}{V_{max}}]\rho_{SOA}, \qquad (3)$$

where $t_{V_{max}}$ is the corresponding time at the maximum particle wall-loss corrected total aerosol volume concentration. V_s is the average particle wall-loss corrected seed volume concentration before the beginning of each experiment. ρ_{SOA} is the SOA density, assumed to be equal to 1.4 µg m^{-3} (Kostenidou et al., 2007). Ideally, V(t) should equal to V_{max} after the reactions are completed and particle wall loss is the only process after $t_{V_{max}}$. However, deviations of $V(t)$ from V_{max} are caused by the uncertainty associated in applying the size-dependent wall-loss corrections. By scaling V_s with $V(t)/V_{max}$, we are distributing the impact of any potential fluctuations in $V(t)$ evenly to both the seeds and the organics, and thus obtain a more stable C_{SOA} after aging.

8

Atmospheric
Chemistry
and Physics
Discussions

3.3 Analysis of AMS measurements

242

243   The HR-AMS was operated in V mode during the experiments in this work. Squirrel

244 v1.56D was used to analyze the data. The atomic oxygen to carbon ratio, O:C, was determined

245 based on the unit-resolution correlation described in Caragaratna et al. (2015). Nitrate signals were

246 attributed to organics since the only sources of them in these experiments are organonitrate

247 compounds.

248

4. Results and discussion

249

250   The particle wall-loss corrected aerosol number concentration evolution during a typical

251 experiment (Exp. 1) together with the SMPS raw measurements are shown in Fig. 1. Prior to the

252 ozonolysis, 18,000 cm^{-3} ammonium sulfate particles were added to the chamber as seeds. After a

253 4.5 h wall-loss period, 8,000 cm^{-3} particles remained suspended, serving as pre-existing surface

254 for condensation. At t=0, ozone was added into the chamber, reacting with α-pinene to form

255 condensable first-generation products. An additional 100 cm^{-3} particles were formed due to

256 nucleation at this time. Two doses of HONO were added into the chamber in this experiment at

257 t=0.4 h and t=1.3 h, respectively. HONO was allowed to mix in the chamber and then the UV

258 lights were turned on at t=0.8 h and t=1.8 h to produce OH. At t=3.5 h, another 10,000 cm^{-3}

259 ammonium sulfate particles were added into the chamber for a second 4 h long determination of

260 the $k(D_p)$ profile for this experiment.

261   The two $k(D_p)$ profiles determined from the initial seed wall-loss period and the one at the

262 end of the experiment are shown in Fig. 2. They agree relatively well with small discrepancies at

263 $D_p < 50$ nm. The complete $k(D_p)$ profile used for the size-dependent particle wall-loss correction

264 is also shown.

265   As indicated in Fig. 1, the particle wall-loss corrected aerosol number concentration

266 remains relative level at t<0 h and t>3.5 h, with $\varepsilon_{N,1} = 3.3\ \%$ and $\varepsilon_{N,2} = 0.5\ \%$, respectively. The

267 particle wall-loss corrected aerosol volume concentration (Fig. 3) at the initial seed wall-loss

268 period and that at the end had variabilities equal to $\varepsilon_{V,initial} = 4.2\ \%$ and $\varepsilon_{V,end} = 3.8\ \%$,

269 respectively. All parameters were less than 5 % and therefore the accuracy of the wall-loss

270 correction was acceptable.

271   The particle wall-loss corrected aerosol volume concentration evolution for Exp. 1 together

272 with the corresponding SMPS raw measurements are shown in Fig. 3. Particles grew from t=0 to

Atmospheric
Chemistry
and Physics
Discussions

273   0.7 h and t=0.8 to 1 h due to vapor condensation. The total aerosol volume peaked at t=0.7 h during

274   the first-generation oxidation, and reached its maximum at t=1.1 h due to aging during the second-

275   generation oxidation. The change in volume during the second addition of OH at 1.7 h was

276   negligible.

277   The SOA mass concentration evolution for Exp. 1 calculated using Eqn. 3 is shown in Fig.

278   4. The error bars are calculated using the highest ε (in this case $\varepsilon_{V,1} = 4.2$ %). For this experiment,

279   37.7±1.6 µg m^{-3} of SOA was formed during ozonolysis. An additional 11.1±2.6 µg m^{-3} SOA was

280   formed during the first aging period. The SOA reached 48.8±2 µg m^{-3} after aging and remained

281   approximately constant utill the end of the experiment. The total SOA produced and the calculated

282   SOA yields for all experiments are listed in Table 2.

283   The AMS-derived atomic oxygen to carbon ratio (O:C) evolution for Exp. 1 is shown

284   together with the AMS-measured aerosol composition (assuming CE=1) in Fig. 5. The increase in

285   the sulfate signals at t=0 is caused by a change in the instrument collection efficiency. Due to the

286   uncertainty caused by CE changes over the course of an experiment, we did not use the absolute

287   AMS-measured organic mass concentration for any quantitative analysis. Using the algorithm

288   derived by Kostenidou et al. (2007), we calculated the CE to be ~0.25 for the initial seed period

289   and ~0.4 after the seeds were coated with organics. A quick check comparing the two stepwise

290   increase in the CE-corrected organic mass concentration to those derived from SMPS revealed that

291   the results from both instrument agreed reasonably well.

292   The O:C is a collective measure for the ongoing chemistry during these aging experiments.

293   In Exp. 1, the O:C kept decreasing due to the freshly-formed semi-volatile SOA condensing onto

294   particles from t=0 to 0.5 h. From t=0.5 h to 0.8 h (UV on), the O:C ratio kept decreasing to 0.42

295   while the organic mass concentration stayed almost constant. This is consistent with the "ripening"

296   phenomenon, first observed during the MUCHACHAS campaign, where the composition of the

297   formed SOA keeps evolving after α-pinene has reacted while the change in SOA mass is minimal

298   (Tritscher et al., 2011). After OH radicals were generated in the chamber at t=0.8 h, the semi-

299   volatile vapors got oxidized to form second-generation products of lower volatility, resulting in an

300   increase of 0.02 in O:C in about 10 min. After t=1 h, the O:C remained relatively constant but it

301   started to decrease at t=1.25 h when the UV lights were turned off. Since aging is a complex

302   process that involves functionalization, fragmentation and heterogeneous reactions, the trends in

303   O:C are indicative of the competition among these processes. The decrease we observed here was

Atmospheric
Chemistry
and Physics
Discussions

304   associated with turning the UV lights off, and thus it is likely that some chemistry was perturbed

305   and thus the processes resulting in decreasing O:C took over. The decrease in O:C associated with

306   turning off the UV lights was not consistent across the five experiments. This further proves that

307   this phenomenon is the result of several competing process and needs further investigation on a

308   molecular level. An inflection point at t=1.7 h was observed after a second dose of OH being

309   introduced in the chamber. Instead of the stepwise increase like the one observed after the first

310   dose of OH, the O:C increased slowly but steadily this time until the end of the experiment to 0.45

311   with no significant increase in organic mass. This is also quite consistent with what was observed

312   in MUCHACHAS.

313   We used the organic to sulfate ratio (Org/Sulf) derived from AMS measurements to look

314   at the SOA formation in these experiments due to its insensitivity to changes in collection

315   efficiency. The Org/Sulf time series for Exp. 1 is shown in Fig. 6. The ratio increased to 1.25 at

316   t=0.7 h as the result of the first-generation vapors condensing onto pre-existing particles. After we

317   first turned on the UV lights, a stepwise increase in the ratio was observed and reached the

318   maximum value of 1.60 at t=1.1 h as a result of the second-generation oxidation chemistry. After

319   that, the ratio kept decreasing. A small bump was observed after the second introduction of OH

320   and then the ratio kept decreasing. One possible explanation for this continuous decrease is the

321   effect of the size-dependent particle wall-loss process. The faster removal of smaller particles

322   (which contain more SOA than sulfate) than that of the bigger ones (which have a lower SOA to

323   sulfate ratio) can lead to a decrease of the overall organic to sulfate ratio. Fig. 7 shows the size

324   dependence of the Org/Sulf, together with the mass distribution of both organic and sulfate for

325   Exp. 1. The Org/Sulf decreased dramatically from 10 to 1 over the particle vacuum aerodynamic

326   diameter (D_{va}) range of 200 – 500 nm, indicating strong composition dependence on particle size.

327   Since the majority of the mass is distributed in this range, the size-dependent particle wall-loss rate

328   can contribute significantly to the decrease observed in Fig. 6 after the Org/Sulf reached its

329   maximum.

330

4.1 Effect of size-dependent losses on the organic to sulfate ratio

332   To quantify the effect of the size-dependence of the particle wall-loss process on the

333   organic to sulfate ratio, we discretized the AMS-measured mass distribution $M(D_p)$ into 10 bins

Atmospheric
Chemistry
and Physics
Discussions

334   in the particle diameter space and defined a mass-weighted particle wall-loss rate constant for each

335   species j, $\bar{k}_j$, as

336

337    $$\bar{k}_j = \sum_{i=1}^{10} M_{ij} k_i \,/\, \sum_{i=1}^{10} M_{ij} \qquad (4)$$

338

339   where M_{ij} is the aerosol mass concentration of species j for size bin i and k_i is the averaged $k(D_p)$

340   across size bin i. Note that the particle diameter used in this section refers to the SMPS-measured

341   mobility equivalent diameter D_p. The particle vacuum aerodynamic diameters derived from the

342   AMS measurements have been converted to D_p using an SOA density of 1.4 µg m^{-3}.

343   From Eqn. 4 we are able to determine a mass-weighted particle wall-loss rate constant for

344   sulfate, $\bar{k}_{SO_4}$, and for organics, $\bar{k}_{Org}$. For the period after completion of the reactions and if there

345   are only particle losses to the walls the Org/Sulf ratio should satisfy:

346

347    $$(\mathrm{Org/Sulf})(t) = (\mathrm{Org/Sulf})_m(t)\exp\left(\bar{k}_{SO_4} - \bar{k}_{Org}\right)t \qquad (5)$$

348

349   where $(\mathrm{Org/Sulf})_m(t)$ is the AMS-measured and $(\mathrm{Org/Sulf})(t)$ the loss-corrected organic to

350   sulfate ratio.

351   We can test if indeed the particle wall losses are responsible for the decreasing ratio in Exp.

352   1 focusing on the period from $t_1 = 1.2$ h to $t_2 = 1.7$ h (Fig. 6). In this example t_1 corresponds to

353   the maximum Org/Sulf and t_2 is the second time in which the UV lights were turned on. Applying

354   Eqn. 4, we found the mass-weighted particle wall-loss rate constant for organics, $\bar{k}_{Org} = 0.06\ h^{-1}$,

355   and for sulfate, $\bar{k}_{SO_4} = 0.05\ h^{-1}$. The black line in the inset graph of Fig. 6 indicates the particle

356   wall-loss corrected Org/Sulf for the chosen time period using Eqn. 5. The loss-corrected ratio

357   remained relatively constant indicating that the size-dependent particle wall-loss process coupled

358   with the different size distributions of the sulfate and organics were causing the decrease in the

359   ratio. This exercise was repeated for the other experiments arriving in the same conclusion.

360

361   **4.2 Effect of chemical aging on additional SOA formation**

362   To quantify aging effects based on the SMPS measurements, we define the fractional

363   change in the particle wall-loss corrected SOA mass concentration after aging, $\Delta[OA]$, as:

Atmospheric
Chemistry
and Physics
Discussions

364 $$\Delta[OA] = (C_{SOA,2} - C_{SOA,UV})/C_{SOA,1}, \tag{6}$$

366 where $C_{SOA,UV}$ is the particle wall-loss corrected aerosol mass concentration at the time when we

367 first turned on the UV lights. $C_{SOA, UV}$ can be equal to $C_{SOA,1}$ depending on how level the first-

368 generation SOA mass concentration remains after wall-loss correction. Fig. 8 summarizes the

369 $\Delta[OA]$ for all five experiments with the values and corresponding errors listed in Table 2. The OH

370 exposure resulted in an average increase of 24±6 % in SOA mass concentration after aging, ranging

371 from 20 to 29 %. Our HONO injection method creates OH levels of about 2.4×10^7 molecules

372 cm^{-3} for the first hour and then the concentration dropped to around 5×10^6 molecules cm^{-3}. The

373 OH exposure is equivalent to 2-4 days of typical atmospheric oxidation conditions, assuming an

374 OH concentration of 2×10^6 molecules cm^{-3}. The uncertainties displayed in Fig. 8 were propagated

375 from uncertainties in the SOA mass concentration.

376 To quantify aging effects based on the AMS data, we define the fractional change in the

377 organic to sulfate ratio:

379 $$\Delta[Org/Sulf] = ([Org/Sulf]_2-[Org/Sulf]_{UV})/[Org/Sulf]_1, \tag{7}$$

381 where $[Org/Sulf]_{UV}$ refers to the organic to sulfate ratio at the time when we first turned on the UV

382 lights, $[Org/Sulf]_1$ the maximum before we first turned on the UV lights and $[Org/Sulf]_2$ the

383 maximum after the OH exposure. Fig. 8 summarizes the $\Delta[Org/Sulf]$ calculated for all five

384 experiments with the values and corresponding errors listed in Table 2. The uncertainties are based

385 on the deviation between the measured and the corrected Org/Sulf (Fig. 6 inset) over the chosen

386 time period. An associated error is calculated respectively for $[Org/Sulf]_{UV}$, $[Org/Sulf]_1$ and

387 $[Org/Sulf]_2$. The reported error for $\Delta[Org/Sulf]$ in Table 2 is the propagated results of the three.

388 For experiments in this work, the percent increase in organic to sulfate ratios ranged from 18 to

389 27 % with an average increase of 21±4 %. The values are fairly consistent with the SMPS-derived

390 $\Delta[OA]$.

4.2.1 Role of RH

393 Exp. 5, performed at the intermediate RH of 50 %, resulted in a comparable change in SOA

394 formation after aging as experiments at lower RH (Fig. 8). In this experiment, the increase in

Atmospheric
Chemistry
and Physics
Discussions

395 Org/Sulf after aging was 21.2 %, 1.5 % higher than the average Δ[Org/Sulf] of experiments 2-4.

396 Δ[OA] for Exp. 5 was 20.5 %, about 2 % lower than the average Δ[OA] of experiments 2-4. The

397 effect of RH on the SOA formation during chemical aging, at least for these conditions, appears

398 to be small.

399

400 **4.2.2 Role of organic vapor loss to the Teflon walls**

401   For chamber SOA experiments with preexisting particles, the particles act as competing

402 surface against the chamber walls. We calculated the condensation sink (CS) of particles using the

403 method described in Trump et al. (2014) with a unit accommodation coefficient, consistent with

404 recent findings (Julin et al., 2014; Palm et al., 2016). The calculated condensation sink in the form

405 of time scale for vapors condensing onto particles (1/CS) for Exp. 1 is shown in Fig. 9. During the

406 entire experiment, the timescale for vapors to condense onto particles remained less than a minute.

407 Compared to the organic vapor wall-loss timescale of 15 min in the CMU chamber (Ye et al.,

408 2016), the vapors condense onto the particles 15 times faster than that onto the walls. This

409 corresponds to a 6.3 % loss of the semi-volatile vapors to the walls. For the experiments conducted

410 in this work, the yields should be increased by 1-3 % after accounting for the vapor wall-loss effect.

411   The situation is a little more complex for the second-generation oxidation because material

412 with higher volatilities that could have become SOA were lost during the time after the end of the

413 first phase and before the beginning of the second. To address this issue, OH radicals were

414 introduced about an hour earlier in Exp. 1 as compared to the rest of the experiments. A shorter

415 timescale ensures the first-generation vapor products react efficiently with OH instead of

416 interacting with the chamber walls as in the case of longer timescales. There was an increase of

417 27 % in Org/Sulf in this experiment after aging, 7 % more than the average of the other four

418 experiments. Δ[OA] for Exp. 1 was 29.4 %, about 7.5 % higher than the average of the rest four

419 experiments. If we attribute this 7 % difference purely to the vapor wall-loss effect, then we

420 estimate that vapor losses can increase the additional SOA formation by roughly another 10 % for

421 the experiments conducted in this work.

422

423 **4.3 Effect of chemical aging on O:C**

424   Fig. 10 summarizes the absolute increase in O:C after the two doses of OH, respectively,

425 with the corresponding exposure required to achieve the increase. As we discussed above using

Atmospheric
Chemistry
and Physics
Discussions

426   Exp. 1 as an example, the O:C in all experiments showed a stepwise increase after the first OH

427   introduction while it grew continuously after the second OH introduction until the end of the

428   experiment. For these five experiments, it took 10 - 30 min for the O:C to increase by 0.02-0.04.

429   The stepwise increase in O:C is caused by the rapid reactions between the first generation vapor

430   products and the OH. One of the major products identified in the gas phase from the α-pinene

431   ozonolysis system, pinonaldehyde, reacts with OH at a rate of 4.4×10^{-11} cm^3 molecule^{-1} s^{-1}

432   (Atkinson and Arey, 2003). During the first hour of OH introduction, the OH concentration

433   remains on average at a steady state of 2.4×10^7 molecule cm^{-3}. A quick estimation of $1/k_{OH}[OH]$

434   gives a timescale of 16 min, which is consistent with what we observed in these experiments. The

435   second exposure corresponds to the period until the end of each experiment. The increase in O:C

436   of 0.01 to 0.04 clearly indicates change in SOA composition, however paired with minimum

437   change in SOA mass. This phenomenon is likely caused by heterogeneous reactions.

438

439   **4.4 Comparison with other studies**

440   Overall, the results from our chamber experiments in this work are consistent to those from

441   the MUCHACHAS chambers. After adopting a size-dependent particle wall-loss correction

442   method, we observed 20-30 % additional SOA formation after aging. Vapor wall-loss effect can

443   account for an additional 10 %, increasing the range to 20-40 %. The O:C presented a stepwise

444   increase of 0.02-0.04 after the first introduction of OH, and then increased gradually overtime after

445   the second introduction of OH.

446   During the MUCHACHAS campaign, mixtures of SOA and gas-phase products formed in

447   the Paul Scherrer Institute (PSI) 27 m^3 Teflon chamber from low (10 ppb) and high (40 ppb) initial

448   α-pinene concentration were exposed to OH by TME ozonolysis and HONO photolysis at an RH

449   of approximately 50 % (Tritscher et al. 2011). An OH concentration of 2×10^6 to 10×10^6 molecules

450   cm^{-3} was maintained up to four hours. The authors reported an additional 50 % SOA mass forming

451   after aging using the first-order, size-independent particle wall-loss correction for the suspended

452   organic mass concentration measured by AMS. An increase of 0.04 in the oxygen to carbon ratio

453   was also observed during aging.

454   In the 84.5 m^3 Aerosol Interaction and Dynamics in the Atmosphere (AIDA) aluminum

455   chamber at Karlsruhe Institute of Technology, an OH concentration of 2×10^6 to 10×10^6 molecules

456   cm^{-3} was used by a constant flow of TME (dark aging). The authors observed an increase of 17-

Atmospheric
Chemistry
and Physics
Discussions

457   55 % in the SMPS-derived SOA mass concentration (density corrected) after aging during four

458   experiments with initial α-pinene concentration ranging from 14 to 56 ppb (Salo et al., 2011). In

459   the 270 m^3 Simulation of Atmospheric Photochemistry in a large Reaction (SAPHIR) Teflon

460   chamber at Forchungzentrum Jülich, SOA and vapors generated from the ozonolysis of 40 ppb α-

461   pinene was aged for three consecutive days with OH produced by ambient light chemistry. An OH

462   concentration of 2-5×10^6 molecules cm^{-3} was maintained and 9 %, 4 % and 1 % additional SOA

463   was formed respectively after aging each day. These values were corrected for particle wall loss

464   using different wall-loss rate constants determined during different periods of the experiment.

465   Our result of 20-40 % additional SOA formation due to aging is well within the range of

466   that from the above chambers. The difference in the results from each chamber could potentially

467   be attributed to different OH exposure (e.g. a constant flow of HONO or TME was provided in the

468   PSI chamber). Other plausible explanations include whether the reported values were particle wall-

469   loss corrected and whether the same method was adopted for the correction.

470   For the HONO aging experiment performed in the CMU chamber during the

471   MUCHACHAS campaign, Henry and Donahue (2012) suggested a potentially strong photolysis

472   effect based on decreasing organic to sulfate ratio derived from the AMS measurements. In our

473   experiments, the organic to sulfate ratio was affected by the size-dependent wall-loss process. Both

474   the AMS-measured organic to sulfate ratio and the SMPS-measured OA remained relatively

475   constant after correcting for the size dependence of the particle-wall process in these experiments.

476   We thus conclude that minimum photolysis was observed for our experiments.

477

478   **5. Conclusions**

479   With an OH exposure equivalent to 2-4 days of typical atmospheric oxidation conditions,

480   the OH aging of the α-pinene ozonolysis products formed 20-40 % additional SOA mass for the

481   experimental conditions used in this work. Elevated RH up to 50 % has minimum effect on SOA

482   production due to aging. We have constrained the aging effects on additional SOA formation

483   quantitatively using both SMPS and AMS measurements.

484   A more oxygenated product distribution was observed after aging. A stepwise increase of

485   0.02-0.04 in O:C was observed within half an hour after the first introduction of OH. After the

486   second-generation products were exposed to additional OH, the O:C grew continuously until the

487   end of the experiments with an absolute increase of up to 0.04. During this period, minimum SOA

Atmospheric
Chemistry
and Physics
Discussions

488   production was observed. We attribute this phenomenon to condensed-phase reactions. Further

489   investigation on a molecular scale is needed.

490

493

494   **6. References**

495   Atkinson, R., and Arey J.: Atmospheric degradation of volatile organic compounds, Chemical
496   Reviews, 103, 4605-4638, 2003.
497   Barmet, P., Dommen, J., DeCarlo, P. F., Tritscher, T., Praplan, A. P., Platt, S. M., Prévôt A. S.
498   H., Donahue, N. M., and Baltensperger, U.: OH clock determination by proton transfer
499   reaction mass spectrometry at an environmental chamber, Atmos. Meas. Tech., 5, 647–656,
500   2012.
501   Canagaratna, M. R., Jimenez, J. L., Kroll, J. H., Chen, Q., Kessler, S. H., Massoli, P., Hildebrandt
502   Ruiz, L., Fortner, E., Williams, L. R., Wilson, K. R., Surratt, J. D., Donahue, N. M., Jayne,
503   J. T., and Worsnop, D. R.: Elemental ratio measurements of organic compounds using
504   aerosol mass spectrometry: characterization, improved calibration, and implications,
505   Atmos. Chem. Phys., 15, 253-272, 2015.
506   Chacon-Madrid, H. J., Henry, K. M., and Donahue, N. M.: Photo-oxidation of pinonaldehyde at
507   low NO$_x$: from chemistry to organic aerosol formation, Atmos. Chem. Phys., 13, 3227-
508   3236, 2013.
509   Cocker III, D. R., Flagan, R. C., and Seinfeld, J. H.: State-of-the-art chamber facility for studying
510   atmospheric aerosol chemistry, Environ. Sci. Technol., 35, 2594–2601, 2001.
511   Crump, J. G., and Seinfeld, J. H.: Turbulent deposition and gravitational sedimentation of an
512   aerosol in a vessel of arbitrary shape, J. Aerosol Sci., 2, 405–415, 1981.
513   Davidson, C. I., Phalen, R. F., and Solomon, P. A.: Airborne particulate matter and human health:
514   a review, Aerosol Science and Technology, 39, 737–749, 2005.
515   Donahue, N. M., Henry, K. M., Mentel, T. F., Kiendler-Scharr, A., Spindler, C., Bohn, B., Brauers,
516   T., Dorn, H. P., Fuchs, H., Tillmann, R., Wahner, A., Saathoff, H., Naumann, K.-H.,
517   Mohler, O., Leisner, T., Muller, L., Reinnig, M.-C., Hoffmann, T., Salo, K., Hallquist, M.,
518   Frosch, M., Bilde, M., Tritscher, T., Barmet, P., Praplan, A. P., DeCarlo, P. F., Dommen,
519   J., Prevot, A. S. H., and Baltensperger, U.: Aging of biogenic secondary organic aerosol
520   via gas-phase OH radical reactions, Proc. Natl. Acad. Sci., U.S.A., 109, 13503 −13508,
521   2012.
522   Donahue, N. M., Robinson, A. L., Stanier, C. O., and Pandis, S. N.: Coupled partitioning, dilution
523   and chemical aging of semivolatile organics, Environ. Sci. Technol., 40, 2635-2643, 2006.
524   George, I. J., Slowik J., and Abbatt J. P. D.: Chemical aging of ambient organic aerosol from
525   heterogeneous reaction with hydroxyl radicals, Geophys. Res. Lett., 35, L13811, 2008.
526   Griffin, R. J., Cocker, D. R., Seinfeld, J. H., and Dabdub, D.: Estimate of global atmospheric
527   organic aerosol from oxidation of biogenic hydrocarbons, Geophys. Res. Lett., 26, 2721–
528   2724, 1999.

529   Henry, K. M., and Donahue, N. M.: Photochemical aging of α-pinene secondary organic aerosol:
530   effects of OH radical sources and photolysis: J. Phys. Chem. A, 116, 5932−5940, 2012.
531   Henry, K. M., Lohaus T., and Donahue, N. M.: Organic aerosol yields from α-pinene oxidation:
532   bridging the gap between first-generation yields and aging chemistry, Environ. Sci.
533   Technol., 46, 12347−12354, 2012.
534   Intergovernmental Panel on Climate Change: Climate Change 2007: Synthesis Report.
535   Contribution of Working Groups I, II and III to the Fourth Assessment Report of the
536   Intergovernmental Panel on Climate Change, edited by R. K. Pachauri and A. Reisinger,
537   eds., 104 pp., Cambridge Univ. Press, New York, 2007.
538   Julin, J., Winkler, P. M., Donahue, N. M., Wagner, P. E., and Riipinen, I.: Near-unity mass
539   accommodation coefficient of organic molecules of varying structure, Environ. Sci.
540   Technol., 48, 12083–12089, 2014.
541   Kalberer, M., Sax, M., and Samburova, V.: Molecular size evolution of oligomers in organic
542   aerosols collected in urban atmospheres and generated in a smog chamber, Environ. Sci.
543   Technol., 40, 5917−5922, 2006.
544   Keywood, M. D., Varutbangkul, V., Bahreini, R., Flagan, R. C., and Seinfeld, J. H.: Secondary
545   organic aerosol formation from the ozonolysis of cycloalkenes and related compounds,
546   Environ. Sci. Technol., 38, 4157–4164, 2004.
547   Krechmer, J. E., Pagonis, D., Ziemann, P. J., and Jimenez, J. L: Quantification of gas-wall
548   partitioning in Teflon environmental chambers using rapid bursts of low-volatility oxidized
549   species generated in situ, Environ. Sci. Technol., 50, 5757–5765, 2016.
550   Kostenidou E., Pathak R. K., and Pandis S. N.: An algorithm for the calculation of secondary
551   organic aerosol density combining AMS and SMPS data; Aerosol Science and Technology,
552   41, 1002–1010, 2007.
553   Lambe, A. T., Miracolo, M. A., Hennigan, C. J., Robinson, A. L., and Donahue, N. M.: Effective
554   rate constants and uptake coefficients for the reactions of organic molecular markers (n-
555   alkanes, hopanes and steranes) in motor oil and diesel primary organic aerosols with
556   hydroxyl radicals, Environ. Sci. Technol., 43, 8794−8800, 2009.
557   Lane, T., Donahue, N. M., and Pandis, S. N.: Simulating secondary organic aerosol formation
558   using the volatility basis-set approach in a chemical transport model, Atmospheric
559   Environment, 42, 7439-7451, 2008.
560   Loza, C. L., Chhabra, P. S., Yee, L. D., Craven, J. S., Flagan, R. C., and Seinfeld, J. H.: Chemical
561   aging of m-xylene secondary organic aerosol: laboratory chamber study, Atmos. Chem.
562   Phys., 12, 151–167, 2012.
563   Matsunaga, A., and Ziemann, P. J.: Gas-wall partitioning of organic compounds in a Teflon film
564   chamber and potential effects on reaction product and aerosol yield measurements, Aerosol
565   Science and Technology, 44, 881–892, 2010.
566   McMurry, P. H., and Rader, D. J.: Aerosol wall losses in electrically charged chambers, Atmos.
567   Chem. Phys., 4, 249–268, 1985.
568   Müller, L., Reinnig, M. C., Naumann, K. H., Saathoff, H., Mentel, T. F., Donahue, N. M., and
569   Hoffmann, T.: Formation of 3-methyl-1,2,3-butanetricarboxylic acid via gas phase
570   oxidation of pinonic acid - a mass spectrometric study of SOA aging, Atmos. Chem. Phys.,
571   12, 1483–1496, 2012.
572   Nah, T., McVay, R. C., Zhang, X., Boyd, C. M., Seinfeld, J. H., and Ng, N. L.: Influence of seed
573   aerosol surface area and oxidation rate on vapor wall deposition and SOA mass yields: a
574   case study with α-pinene ozonolysis, Atmos. Chem. Phys., 16, 9361–9379, 2016.

575 Ng, N. L., Kroll, J. H., Chan, A. W. H., Chhabra, P. S., Flagan, R. C., and Seinfeld, J. H.: Secondary
576   organic aerosol formation from m -xylene, toluene, and benzene, Atmos. Chem. Phys., 7,
577   3909–3922, 2007.
578 Palm, B. B., Campuzano-Jost, P., Ortega, A. M., Day, D. A., Kaser, L., Jud, W., Karl, T., Hansel,
579   A., Hunter, J. F., Cross, E. S., Kroll, J. H., Peng, Z., Brune, W. H., and Jimenez, J. L.: In
580   situ secondary organic aerosol formation from ambient pine forest air using an oxidation
581   flow reactor, Atmos. Chem. Phys., 16, 2943–2970, 2016.
582 Pope, C. A., Ezzati, M., and Dockery, D. W.: Fine-particulate air pollution and life expectancy in
583   the United States, New Engl. J. Med., 360, 376-386, 2009.
584 Qi, L., Nakao, S., and Cocker, D. R.: Aging of secondary organic aerosol from α-pinene ozonolysis:
585   Roles of hydroxyl and nitrate radicals, Journal of the Air & Waste Management
586   Association, 62, 1359–1369, 2012.
587 Robinson, A. L., Donahue, N. M., Shrivastava, M. K., Weitkamp, E. A., Sage, A. M., Grieshop,
588   A. P., Lane, T. E., Pierce, J. R., and Pandis, S. N.: Rethinking organic aerosol: semivolatile
589   emissions and photochemical aging, Science, 315, 1259–1262, 2007.
590 Salo, K., Hallquist, M., Jonsson, Å. M., Saathoff, H., Naumann, K.-H., Spindler, C., Tillmann R.,
591   Fuchs, H., Bohn, B.; Rubach, F., Mentel, T. F., Müller, L., Reinnig, M., Hoffmann, T., and
592   Donahue, N. M.: Volatility of secondary organic aerosol during OH radical induced ageing;
593   Atmos. Chem. Phys., 11, 11055–11067, 2011.
594 Tritscher, T., Dommen, J., DeCarlo, P. F., Gysel, M., Barmet, P. B., Praplan, A. P., Weingartner
595   E., Prévôt, A. S. H., Riipinen, I., Donahue, N. M., and Baltensperger, U.: Volatility and
596   hygroscopicity of aging secondary organic aerosol in a smog chamber, Atmos. Chem.
597   Phys., 11, 11477–11496, 2011.
598 Trump, E. R., Riipinen, I., and Donahue, N. M.; Interactions between atmospheric ultrafine
599   particles and secondary organic aerosol mass: a model study, Boreal Environ. Res., 19,
600   352–362, 2014
601 Tsimpidi, A. P., Karydis, V. A., Zavala, M., Lei, W., Bei, N., Molina, L., and Pandis, S. N.: Sources
602   and production of organic aerosol in Mexico City: insights from the combination of a
603   chemical transport model (PMCAMx-2008) and measurements during MILAGRO, Atmos.
604   Chem. Phys., 11, 5153−5168, 2011.
605 Wang, N., Donahue, N. M., and Pandis, S.N.: Performance of different particle wall-loss correction
606   methods for aging experiments of alpha-pinene SOA in a smog chamber, Aerosol Science
607   and Technology; in preparation.
608 Ye, P., Ding, X., Hakala, J., Hofbauer, V., Robinson, E. S., and Donahue, N. M.: Vapor wall loss
609   of semi-volatile organic compounds in a Teflon chamber, Aerosol Science and Technology,
610   50, 822-834, 2016.
611 Zhang, Q., Jimenez, J. L., Canagaratna, M. R., Allan, J. D., Coe, H., Ulbrich, I., Alfarra, M. R.,
612   Takami, A., Middlebrook, A. M., Sun, Y. L., Dzepina, K., Dunlea, E., Docherty, K., De-
613   Carlo, P. F., Salcedo, D., Onasch, T., Jayne, J. T., Miyoshi, T., Shimono, A., Hatakeyama,
614   S., Takegawa, N., Kondo, Y., Schneider, J., Drewnick, F., Borrmann, S., Weimer, S.,
615   Demerjian, K., Williams, P., Bower, K., Bahreini, R., Cottrell, L., Griffin, R. J., Rautiainen,
616   J., Sun, J. Y., Zhang, Y. M., and Worsnop, D. R.: Ubiquity and dominance of oxygenated
617   species in organic aerosols in anthropogenically-influenced Northern Hemisphere
618   midlatitudes, Geophys. Res. Lett., 34, L13801, 2007.

Atmospheric
Chemistry
and Physics
Discussions

619   Zhang, X., Cappa, D. C., Jathar, S. H., McVay, R. C., Ensberg, J. J., Kleeman, M. J., and Seinfeld,
620   J. H.: Influence of vapor wall loss in laboratory chambers on yields of secondary organic
621   aerosol, PNAS, 111, 5802-5807, 2014.
622
623

624

625

626

627

628

Atmospheric
Chemistry
and Physics
Discussions

629

630 **Table 1:** Initial conditions of the α-pinene ozonolysis aging experiments.

631

Experiment	α-pinene (ppb)	O_3 (ppb)	Initial seed surface area (μm^2 cm^{-3})	RH (%)	OH^a ($\times 10^7$ molecules cm^{-3})	OH introduction time (h after α-pinene consumption)
1	33	450	850	<20	2.4	0.3
2	14	600	760	<20	2.7	0.8
3	35	450	720	<20	2.0	1.1
4	16	500	950	<20	2.4^b	1.1
5	20	400	710	~50	2.7	0.8

632

633 [a]The OH concentration was calculated using the decay of butanol-d9 (monitored by PTRMS)

634 (Barmet et al., 2012).

635 [b]Estimated OH concentration for Exp. 4 based on the other experiments. The PTRMS data was

636 not available during that time for Exp. 4.

637

638

639

640

641

642

643

644

645

646

647

648

649

650

651

652

653

Atmospheric
Chemistry
and Physics
Discussions

654
655
656   **Table 2:** SOA mass concentration and yields of the α-pinene ozonolysis aging experiments.
657

Experiment	$C_{SOA,1}$ (μg m^{-3})	Y_1 (%)	$C_{SOA,2}$ (μg m^{-3})	Y_2 (%)	ΔOA (%)	Δ[Org/Sulf] (%)
1	37.7±1.6	20.6±0.9	48.8±2.0	26.7±1.1	29.4±6.9	27.0±5.8
2	16.7±0.9	21.5±1.2	18.3±1.0	23.5±1.3	19.8±8.1	18.1±2.9
3	57.1±1.3	29.4±0.7	71.0±1.6	36.2±0.8	23.5±3.6	19.1±3.6
4	16.8±0.6	19.1±0.6	20.8±0.7	23.7±0.8	24.0±5.3	21.9±2.1
5	22.2±0.7	19.5±0.6	25.4±0.8	22.3±0.7	20.5±4.7	21.2±4.4

658
659
660
661
662
663
664

Atmospheric
Chemistry
and Physics
Discussions
Open Access

665
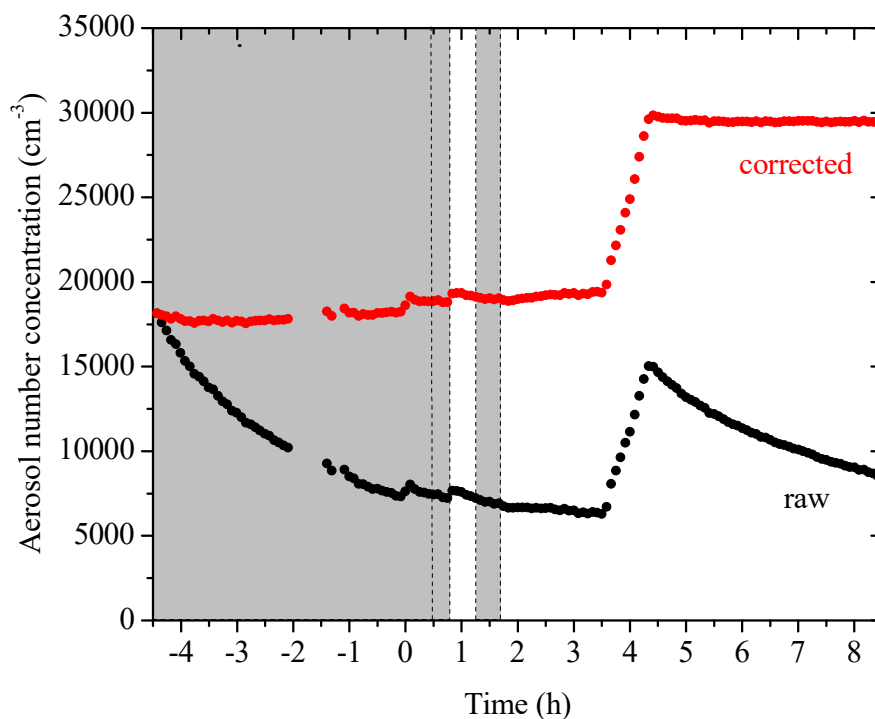
Figure 1: SMPS-measured (black symbols) and the size-dependent particle wall-loss corrected
(red symbols) aerosol number concentration evolution during a typical experiment (Exp. 1). Ozone
was added into the chamber at time zero to initiate α-pinene ozonolysis. The shaded areas indicate
that the chamber was dark. The dashed lines mark the beginning and the end of the two times
HONO were added, respectively. The increase in number concentration at t=3.5 h is due to the
injection of 5 g L^{-1} ammonium sulfate particles. An additional 100 cm^{-3} particles were formed due
to nucleation both at the ozonolysis step and the aging step. Data were not recorded from t = -2 h
to -1.4 h.

674

675

676

Atmospheric
Chemistry
and Physics
Discussions

Open Access

EGU
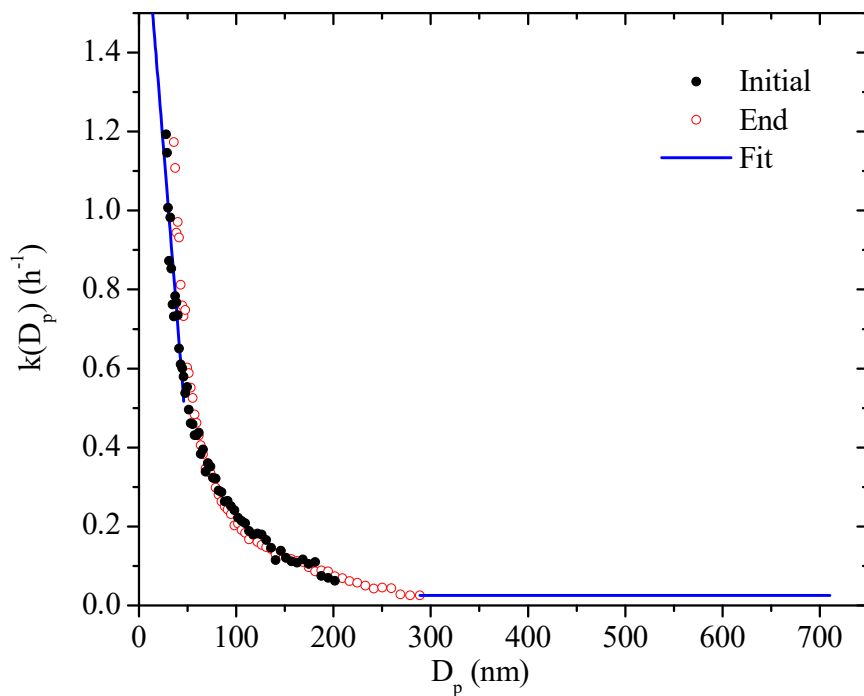
677
Figure 2: The size-dependent particle wall-loss rate constant profile, $k(D_p)$, for Exp. 1. The black
678 symbols are the rate constants calculated based on the wall-loss process of the initial ammonium
679 sulfate seed particles from t=-4.5 h to t=0 h, while the red open symbols that of the additional
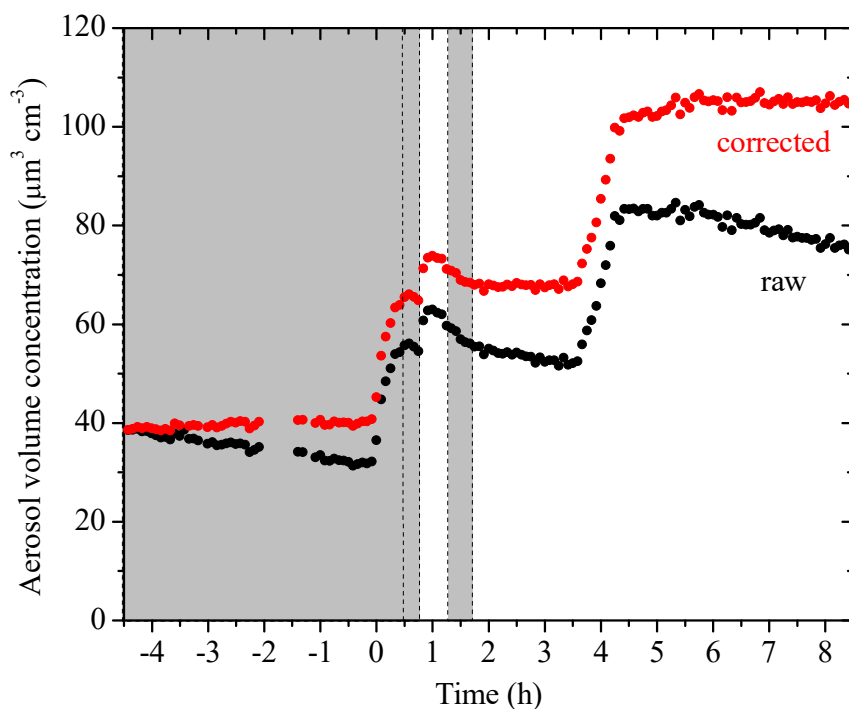680 ammonium sulfate particles at the end from t=4.5 h to t=8.5 h. The blue line is the fit determined.
681
682
683
684
685

Atmospheric
Chemistry
and Physics
Discussions

686

Figure 3: SMPS-measured (black symbols) and the size-dependent particle wall-loss corrected (red symbols) aerosol (seed and organic) volume concentration evolution during a typical experiment (Exp. 1). Ozone was added into the chamber at time zero to initiate α-pinene ozonolysis. The shaded areas indicate that the chamber was dark. The dashed lines mark the beginning and the end of the two times HONO were added, respectively. 5 g L^{-1} ammonium sulfate particles were injected into the chamber at t=3.5 h. Data were not recorded from t=-2 h to -1.4 h.

693

694

Atmospheric
Chemistry
and Physics
Discussions

695
696
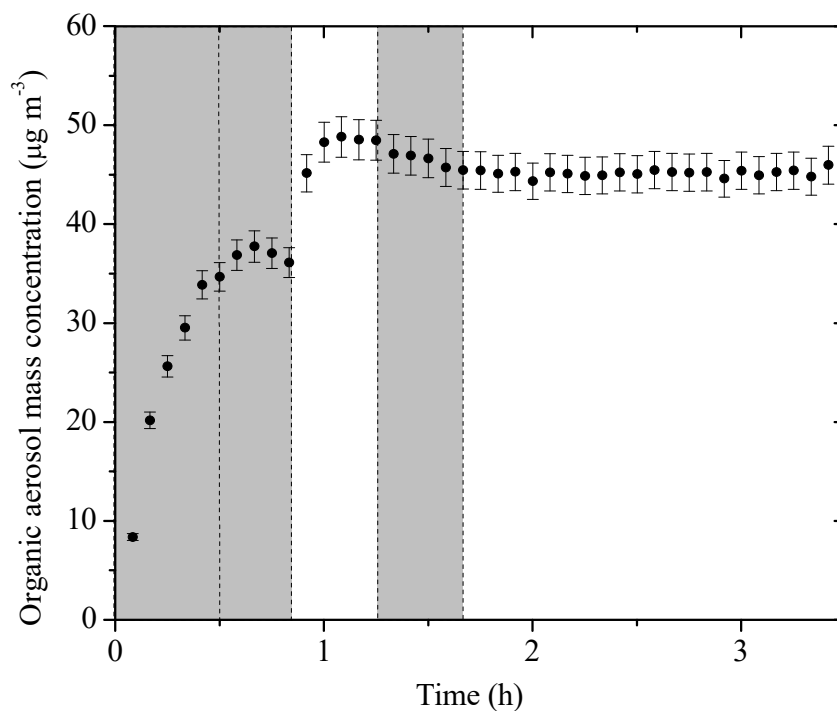
Figure 4: The particle wall-loss corrected SOA mass concentration (ρ=1.4 g cm^{-3}) evolution for
Exp. 1 derived from SMPS measurements. The corresponding error shown is due to the particle
wall-loss correction. Ozone was added into the chamber at time zero to initiate α-pinene ozonolysis.
The shaded areas indicate that the chamber was dark. The dashed lines mark the beginning and the
end of the two times HONO were added, respectively.

702

703
704
705

706

Atmospheric
Chemistry
and Physics
Discussions
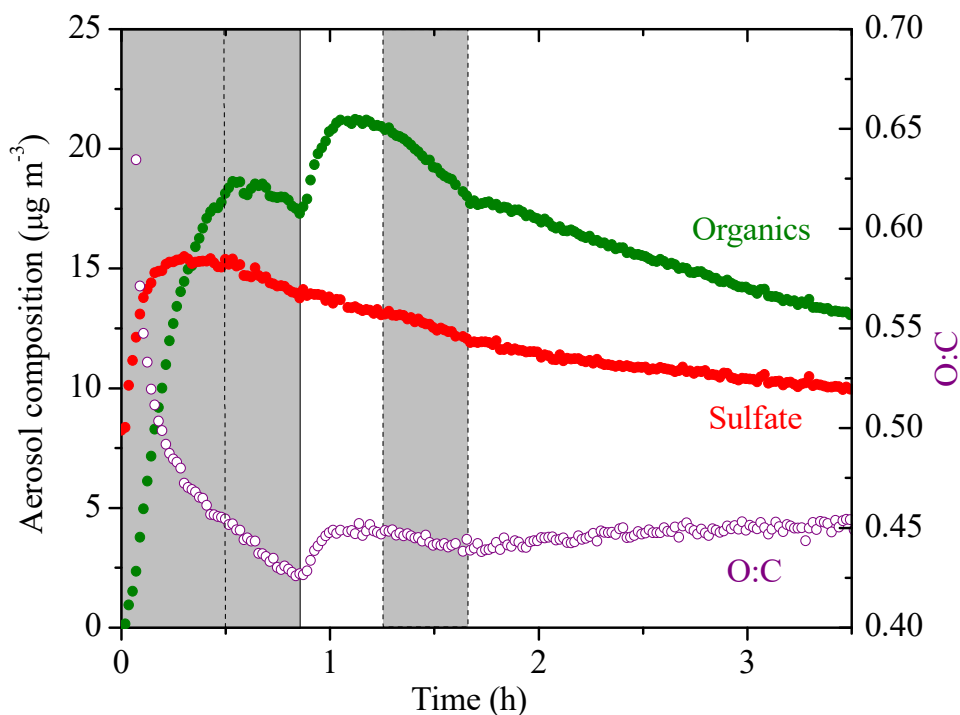
Figure 5: The AMS-measured aerosol composition (CE=1) (left axis) and the atomic oxygen to carbon ratio (right axis) evolving with time for Exp. 4. The increase in the sulfate signal at t=0 is the result of a change in the collection efficiency (CE). Ozone was added into the chamber at time zero to initiate α-pinene ozonolysis. The shaded areas indicate that the chamber was dark. The dashed lines mark the beginning and the end of the two times HONO were added, respectively.
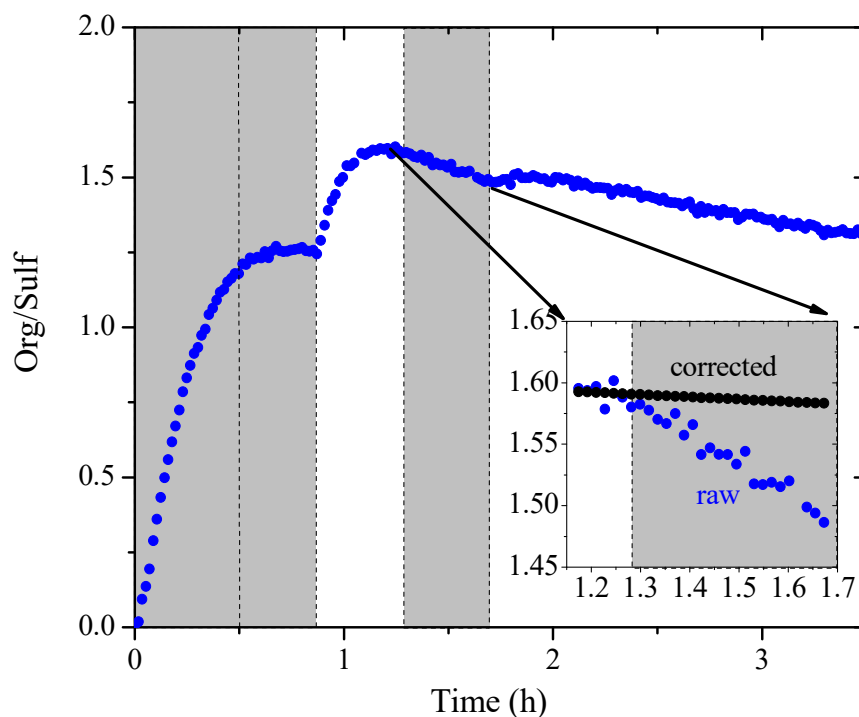
713
714 **Figure 6:** The AMS-derived organic to sulfate ratio time series for Exp. 1. The inset is a blow-up
715 of the Org/Sulf ratio from its maximum until the second time when the UV lights were turned on.
716 The black symbols are the particle wall-loss corrected Org/Sulf during that half hour. Ozone was
717 added into the chamber at time zero to initiate α-pinene ozonolysis. The shaded areas indicate that
718 the chamber was dark. The dashed lines mark the beginning and the end of the two times HONO
719 were added, respectively.

Atmospheric
Chemistry
and Physics
Discussions

720
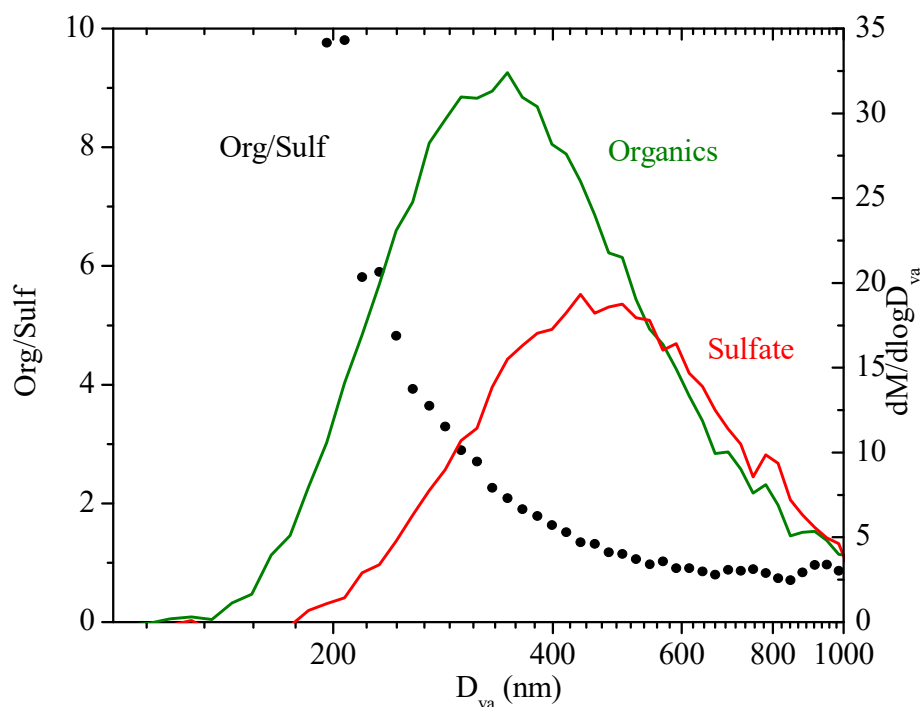
Figure 7: The dependence of the AMS-derived organic to sulfate ratio on particle vacuum
aerodynamic diameter for Exp. 1 (left axis). Also shown are the AMS-measured organic (green)
and sulfate (red) mass distribution (right axis). The results are based on PToF data averaged over
~2.5 hours (t=1.1 h to 3.5 h).

725

726

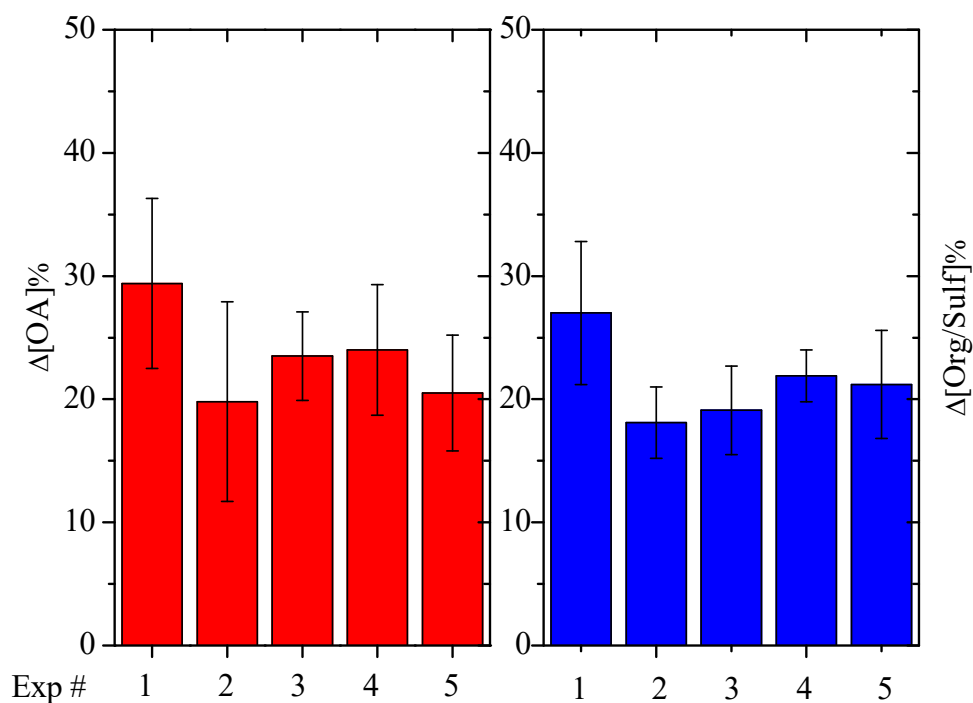727

728

729

730

Atmospheric
Chemistry
and Physics
Discussions

731

732

Figure 8: SMPS-derived percent change in the particle wall-loss corrected SOA (red columns)
mass concentration after aging and AMS-derived percent change in organic to sulfate ratio (blue
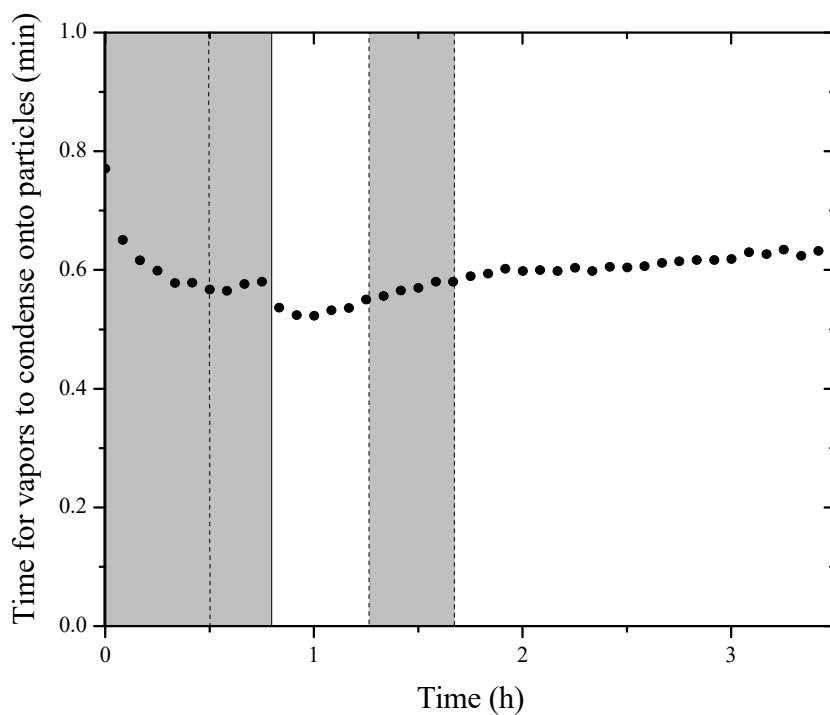columns) after aging for all five experiments.

736

737

738

739

740

741

Atmospheric
Chemistry
and Physics
Discussions

742

Figure 9: The calculated condensation sink (CS) in the form of time scale for vapors condensing onto particles (1/CS). Ozone was added into the chamber at time zero to initiate α-pinene ozonolysis. The shaded areas indicate that the chamber was dark. The dashed lines mark the beginning and the end of the two times HONO were added, respectively.

Atmospheric
Chemistry
and Physics
Discussions
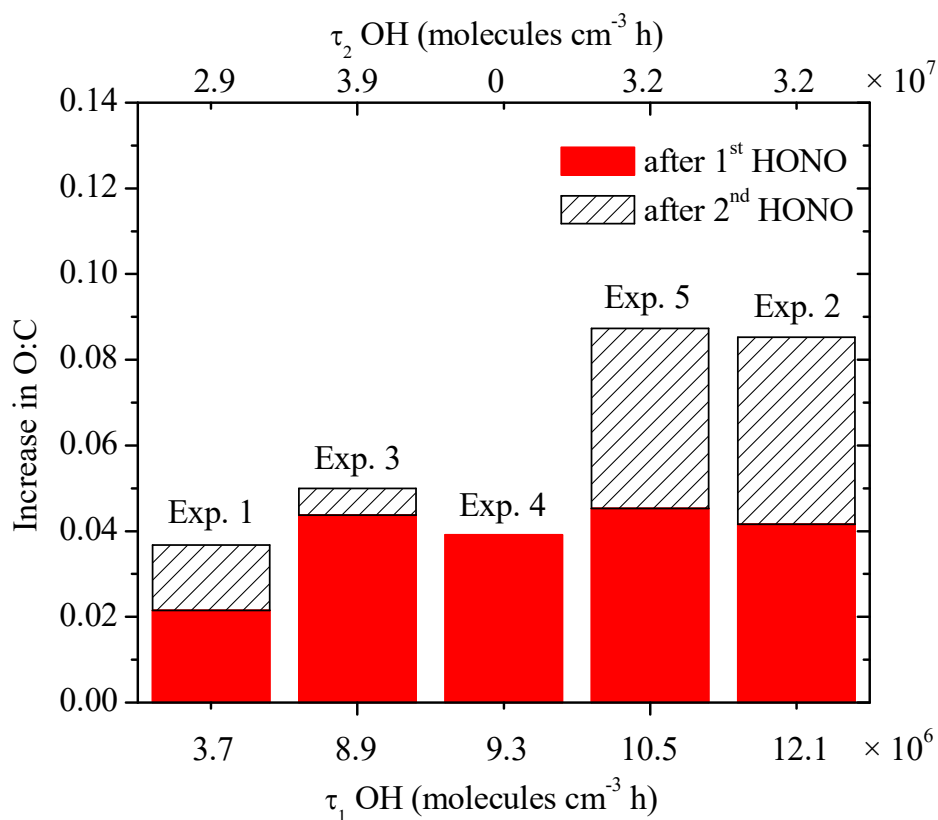
Figure 10: The absolute increase in O:C after the two doses of OH, respectively, with the corresponding exposure. The solid red columns are the increase in O:C after the first introduction of OH, with the corresponding exposure on the bottom axis. The hatched columns are the increase in O:C after the second introduction of OH, with the corresponding exposure on the top axis.